Cyber Security and Applications 2 (2024) 100028

Contents lists available at ScienceDirect

Cyber Security and Applications

journal homepage: http://www.keaipublishing.com/en/journals/cyber-security-and-applications/

Increasing embedding capacity of stego images by exploiting edge pixels in prediction error space

Habiba Sultana [a,*], A.H.M. Kamal [a], Tasnim Sakib Apon [b], Md. Golam Rabiul Alam [b]

[a] Jatiya Kabi Kazi Nazrul Islam University, Mymensingh, 2220, Bangladesh
[b] BRAC University, Dhaka, 1212, Bangladesh

ARTICLE INFO

Keywords:
Edge detection
Predictor
Embedding capacity
PSNR
Steganography
Steganalysis

ABSTRACT

In the field of data concealing, edge detection techniques are frequently employed, particularly for improving image quality and data security. These methods, however, have a lower embedding capacity. In order to take advantage of more edge pixels, many strategies are used nowadays. These schemes either combine the output from multiple edge detectors or enlarge the edges of an edge image by dilating. Even so, if the amount of data is vast, the techniques might not be able to conceal all of it. Therefore, a novel strategy for edge exploitation is still needed to regulate the effectiveness of edge detection-based data-hiding strategies. By using edge detectors in the prediction error space, we utilized more edge pixels in this study (PES). Applying a predictor on the cover image and then calculating the prediction errors, we prepared the PES. The edges in PES were then marked using the edge detector. The edge-error corresponding pixels received more information than the relevant pixels that did not create an edge-error. Additionally, we combined the results from different edge detectors to produce more edges, which does help to achieve a higher embedding capacity. We implanted x number of secret bits in edge pixels and y number of bits in non-edge pixels where $x > y$. The simulation results show that the proposed scheme outperforms its rivals on all performance-measuring criteria, including payload, stego image quality, and resistance to attack.

1. Introduction

Security is an essential part of data communications. There are many techniques in the literature that are currently being used for securing the data. The premier one is cryptography. A cryptography method encrypts the secret messages into an unintelligible format, known as ciphertext, to prevent intruders from realizing the meaning of it [1]. Such meaningless random content in a message, in fact, makes the intruder curious and deeply attentive to look for some hidden meaning in it. Watermarking is another way of securing the message [2]. However, that technique is mainly used for serving data integrity. Additionally, some watermarking methods remain their masks visible on the cover media. Due to those limitations, steganography has taken a firm stand in the field of secured communication. Steganography is a process of hiding data in a cover media, e.g., image, audio, video, text, bio-signals, DNA sequence, etc. [3]. Among these media, images are gaining popularity as a cover media for their higher degree of information redundancy and flexible size for communication over the Internet [4]. In steganography, an embedding technique implants secrets in a cover media. The modified media is called stego media. That stego media is then sent to a destination. The destination end applies an exact de-embedding algorithm to extract the secrets from it. Some de-embedding algorithms, additionally, generate the cover media from the stego one [5–17]. Therefore, all of these methods can be divided into reversible or irreversible depending on their ability to build cover media from stego one.

Intruders can even check if there is something secret in it. In that case, they deal with the possibility of changing cover contents. Such analyses are known as steganalysis techniques [18]. With these considerations in mind, the performance of steganography is evaluated with the ability to increase the data hiding rate, decrease the distortion rate of the carrier and resist attacks.

There are diverse techniques for hiding information in image content. A major part of such algorithms applies edge detection methods [1,2,19–32], as a part of their embedding technique. These schemes find edge and non-edge pixels first and then embed more bits in edge pixels than non-edge ones; because the human visual system is less sensitive to changes in sharp areas of images compared to smooth areas. Such methodology is very useful in yielding both better stego quality and higher data security. However, the embedding capacity depends more on the number of identified edge pixels. The embedding capacity goes high when the number of edge pixels is large.

* Corresponding author.
E-mail address: srity.cse@jkkniu.edu.bd (H. Sultana).

https://doi.org/10.1016/j.csa.2023.100028
Received 15 May 2023; Received in revised form 9 July 2023; Accepted 3 August 2023
Available online 9 August 2023

In 2016, Lee et al. [19] proposed a reversible data hiding method based on reduplicated exploiting modification, image interpolation, and canny edge detection. To enhance the image quality, Kumar et al. [20] proposed a steganography system with fuzzy edge identification and least significant bit (LSB) substitution methods in 2018. S. Sun in 2015 showed another post-processing technique to improve the visual quality of stego images [21]. He applied Huffman encoding to Canny-detected edge pixels to measure the number of bits that could be implanted in each pixel. The method next used a correction method for increasing the visual quality of their stego image. Vanmathi and Prabu in 2017 employed fuzzy logic edge detection method for detecting edge pixels. The authors applied a chaotic method for encrypting messages and the LSB substitution technique for implanting those in edge pixels [22]. G. Swain in 2015 adopted a pixel value difference policy to enhance data security [23]. Uses of Canny, Sobel, and fuzzy as edge detection were compared in [24] in 2017 by Bai et al.. Setiadi in 2022 [25] increased the number of edge pixels by applying morphological operator dilation on edge image owing to improve the edge pixels and thus, the embedding capacity. The author also applied hybrid edge detectors for the same purpose. In addition to the edge detection technique, Kusuuma et al. [26] in 2018 applied an encryption method for the secret message to strengthen the security of hidden data. Khan et al. [27] in 2015 replaced four LSBs of detected edge pixels in their data hiding algorithm. That scheme, indeed, destroyed the image quality roughly. Again, Chen et al. [28] in 2010 combined the results of Canny and Fuzzy edge detectors to exploit more edge pixels. Tseng and Leng in 2014 [29] improved the distortion rate of [28] by working on image blocks rather than the whole image at a time. Link in [25], Gaurav and Ghanekar in 2018 [30] applied a dilation operator to increase the number of edge pixels. They implanted secret bits by applying bit-wise exclusive-OR (XOR) operation between the binaries of each edge pixel and a message chunk. Vishnu et al. in 2020 [31] also used the Canny edge detection method to identify the edge pixels. Next, they computed pixel value differences between each of the two consecutive edge pixels reading in a sequential manner. That pixel value differences were used to implant secret bits in edge pixels. Sultana and Kamal in 2021 [32] employed multiple edge detectors and then measured the desired edge pixels for data hiding by doing a logical AND operation among the pixels of each of the same positions in edge images. That policy is effective for getting better stego quality while the size of the demanded implantable message is small. Setiadi et al. in 2018 [32], combined the results of canny and sobel edge detectors to increase the number of edge pixels.

Studies in the state of the art reveal that edge detection-based embedding schemes suffer from less embedding capacity. Therefore, as the demand for data hiding increases, so does the challenge with the capability of such schemes, because the number of edge pixels obtained in such a conventional way may be unable to conceive the demanded information. Such good methods will then be ineffective. Our target is to enhance the embedding capacity of the edge detection-based steganographic method. For this, we have enriched the edge detection space so that the applied edge detector can detect more edge pixels. To get that, we applied a predictor on the image pixels. We have measured the prediction errors as well. In the prediction error space, we have applied the edge detector. That strategy noticeably increases the number of edge-forming errors in the error space. Corresponding positions of edge and non-edge errors in error space are noted. We have used that positional map to link to the image domain. That mapping is done to classify the image contents as edge and non-edge pixels. We then implant secrets in these pixels by embedding rules. That strategy boosts up the embedding capacity notably. Nevertheless, still, the scheme faces problems in hiding large volumes of data. We further try to increase the number of edge pixels by combining the edge images of multiple edge detectors. Experimental results deduce that the proposed method performs better than the other competing schemes, and shows a noticeable improvement in its capability of hiding more data.

The key contributions of this research are as follows:

- An image steganography approach has been proposed for efficient data hiding on the edges of an image. We have applied edge detectors in prediction error space to increase the embedding capacity of the stego image which signifies the novelty of this research.
- We have adapted the technique of combining the results of multiple edge detectors owing to increase the number of edge pixels, further. We have also made our scheme enable to concealment of a different number of bits in edge and non-edge pixels. Therefore, the proposed scheme increases both the embedding capacity and the visual quality of stego images. At the same time, it shows strong resistance against statistical attacks.

Throughout this manuscript, Section 2 discussed previous existing studies related to this manuscript. Section 3 presents the proposed method neatly. The simulated results of our scheme are demonstrated in Section 4. Section 4.6 is devoted to testing the robustness of the proposed scheme against attacks. Section 5 narrates the implications and limitations of our work. Finally, Section 6 draws a conclusion of the article.

2. Related works

Human visioning systems are sensitive to local changes. In the image, local changes are marked as edges. Edges in the image appear along either horizontal, vertical, or diagonal gradient directions. A filter, known as a kernel, is used to detect the edges in an image. Very commonly used edge detectors are Canny, Sobel, Log, Prewitt, Laplacian, and Fuzzy edge detectors. Now briefly describe those operators in the following:

- Roberts edge detection
  Lawrence Roberts develops the Roberts edge detection (1965). It measures the 2-D spatial gradient of an image in a straightforward and quick manner.

−1	0
0	+1

RG_x

0	−1
+1	0

RG_y

  This technique highlights areas of high spatial frequency, which frequently coincide with edges. The most common application of this approach is when both the input and the output are grayscale images. The estimated full amplitude of the spatial gradient of the input image at each place in the output is represented by the pixel values at each location.
  Robert's cross-operator consists of 2×2 convolution kernels. G_x is a simple kernel and G_y is rotated by 90^0. The gradient magnitude is:

$$|G| = \sqrt{RG_x^2 + RG_y^2} \tag{1}$$

  An approximate magnitude is computed:

$$|G| = |RG_x| + |RG_y| \tag{2}$$

- Sobel edge Detection

−1	−2	−1
0	0	0
+1	+2	+1

SG_x

−1	0	+1
−2	0	+2
−1	0	+1

SG_y

In 1970, Sobel developed the Sobel edge detection method. In order to highlight areas of high spatial frequency that correlate to edges, the Sobel approach performs a $2-D$ spatial gradient quantity on an image. Typically, it is used to determine the predicted absolute gradient magnitude at each location in n input grayscale images. According to the bottom table's disclosure, the operator at the very least is made up of two 3×3 complication kernels. The other kernel is just the first one rotated 90^0. The Roberts Cross operator and this are extremely similar. Sobel Edge detection operator consists of 3×3 convolution kernels. G_x is a simple kernel and G_y is rotated by 90^0. The gradient magnitude is:

$$|G| = \sqrt{SG_x^2 + SG_y^2} \tag{3}$$

An approximate magnitude is computed:

$$|G| = |SG_x| + |SG_y| \tag{4}$$

- Prewitt edge detection
  Prewitt first suggested the Prewitt edge detection in 1970. Prewitt is a reliable method for determining an edge's size and direction. This gradient-based edge detector is estimated in the 3×3 neighborhood for eight directions. Calculations have been made for all eight convolution masks. The next step is to choose one complexity mask, specifically with the largest module in mind.
  The gradient magnitude is:

$$|G| = \sqrt{PG_x^2 + PG_y^2} \tag{5}$$

An approximate magnitude is computed:

$$|G| = |PG_x| + |PG_y| \tag{6}$$

Prewitt detection tends to provide somewhat noisier findings but is computationally slightly easier to execute than Sobel detection.

−1	−1	−1
0	0	0
+1	+1	+1

PG_x

−1	0	+1
−1	0	+1
−1	0	+1

PG_y

- LoG edge detection
  A 2-D isotropic measurement of an image is the Laplacian of Gaussian. Laplacian, which is also utilized for edge detection, is the region of an image that is emphasized and experiences fast intensity variations. To lessen the sensitivity of noise, the Laplacian is applied to an image that has been smoothed using a Gaussian smoothing filter. This operator creates a single grayscale image from a single grayscale image that is input. The input image is represented in Laplacian as a collection of discrete pixels. In order to approach the second derivatives in the definition, a discrete convolution kernel is discovered. The following are the top two kernels:

0	−1	0
−1	4	−1
0	−1	0

LG_x

−1	−1	−1
−1	8	−1
−1	−1	−1

LG_y

The gradient magnitude is:

$$|G| = \sqrt{LG_x^2 + LG_y^2} \tag{7}$$

An approximate magnitude is computed:

$$|G| = |LG_x| + |LG_y| \tag{8}$$

Typically, the Laplacian is employed to determine whether a pixel is on the light or dark side of an edge.

- Canny Edge Detection The Canny edge detection method is one of the common edge detection methods in the industry. It was first designed in 1983 by John Canny for his master's thesis at MIT, and it still outperforms several more recent algorithms. Prior to using the Canny method to locate image edges, it is crucial to remove noise from the image. The Canny approach is superior since it applies the tendency to identify edges and a serious threshold value after preserving the characteristics of the edges in the image. These are the algorithmic steps:
  - A Gaussian filter is used to remove noise from the input image.
  - Calculating the gradient of image pixels in order to determine magnitude along the x and y dimensions.
  - Suppress the non-max edge contributor pixel points while taking into account a cluster of neighbors for any curve pointing in the direction of the specified edge.
  - As a last step, apply the hysteresis thresholding technique to preserve pixels with gradient magnitudes greater than or equal to 1 and exclude pixels with gradient magnitudes less than or equal to 0.

Generally, edge detectors are used in pattern recognition, image morphology, and feature extractions. In the field of image steganography, edge detectors are used to improve the security of hide data as well as to collect the data hiding features. These schemes first detect the edge and non-edge pixels in a cover image. Then these schemes either implant in edge pixels only or embed a different number of bits in edge and non-edge pixels. Bearing that in mind, we studied a good number of articles on that state of the art. Among those, we found the works of Junlan Baiet al. [24] and Setiadi D. R. I. M. [25] which were very close to our research objectives. As a result, we studied these two articles with deep attention and built the foundation of our proposed work on them.

In 2017, Junlan Bai et al. [24] proposed a steganography approach based on the combination of edge detection and LSB substitution methods. In their scheme, the authors first prove that if a few of the LSBs of image pixels are cleared and then an edge detector is applied on that cleared image, let I_clr, the detection information is almost the same as computing edge information by applying the detector in the original image, say I_o. Therefore, they proposed to clear n bits of information in an image before applying an edge detector. They are allowed to implant in the pixels of the cover image by $k - LSB$ substitutions, where $k \leq n$. In practice, they used $n = 5$. Thereafter, they formed stego image I_s by implanting x-bits of information in detected edge pixels and y-bits of information in non-edge pixels, where $x > y$. At the extraction phase, their scheme again cleared n bits of LSBs from stego pixels of I_s. That cleared image is, indeed, I_clr. Hence, the extraction phase feels no ambiguity to detect the same set of edge pixels as the data-hiding phase. The scheme, then, extracts x bits of LSBs from edge pixels and y bits of LSBs from non-edge pixels.

In 2019, Setiadi proposed an image steganography that is very similar to Junlan Bai et al.'s scheme. He also implanted x bits of information in edge pixels and y bits of secrets in non-edge pixels. However, he added some pre-processing tasks to increase the number of edge pixels owing to improving the embedding capacity. He applied multiple edge detectors, say m number of detectors, on 5-LSBs cleared images. These m detectors separately generate m edge images. Let these edge images are I_{e1}, I_{e2}, ..., I_{em}. The scheme increases the number of edge pixels by combining these edge results by doing logical OR operations among the

Table 1
Summary of related works.

Criteria	Bai [24]	Setiadi [25]	Sultana [32]	Rasol [34]	Proposed System
Use an edge detector?	Yes	Yes	Yes	Yes	Yes
Encrypt message?	No	Yes	No	No	No
Cleared LSBs	n-bits	5-bits	n-bits	No	n-bits
Use multi predictors	No	Yes	Yes	Yes	Yes
Hybridize edge image?	No	Yes	Yes	Yes	Yes
Dilate edge image?	No	Yes	No	No	No
Embed as (x, y) bits?	Yes	Yes	Yes	Yes	Yes
Message type?	Binary	Text	Binary	Text	Binary
Use Prediction Error space?	No	No	No	No	Yes

edge images, i.e., by $I_{e1} \vee I_{e2} \vee \ldots \vee I_{em}$. Let the resultant image is rI_e. He dilated the edge image rI_e to increase edge pixels more. He then separated the edge and non-edge pixels from the dilated image.

In 2021, Sultana et al. proposed image steganography based on hybrid edge detectors. In their scheme, the authors applied multiple edge detectors, say p number of detectors, on $m-$ LSBs cleared image, and those detectors separately generated edge images. These edge images are combined using logical AND operations. The authors then implant x bits into edge pixels and y bits into non-edge pixels, where $x > y$.

In 2018, Setiadi proposed image steganography based on canny-Sobel edge detector and LSB substitution methods. In this scheme, the authors applied multiple edge detectors, say m number of detectors, on the cover image. These m detectors separately generate m edge images. Let these edge images be I_1, I_2, ..., I_m. The scheme hybridized those edge images using logical OR operations, i.e., by $I_1 \vee I_2 \vee \ldots \vee I_m$. Let the resultant image is rI_e. As a result, this scheme increases the number of edge pixels. At the same time, the author is added one special character at the end of the secret message then this message is transformed into binary form. The authors then implant x bits into edge pixels and y bits into non-edge pixels (where $x > y$) based on message length.

Table 1 provides a summary of comparisons among the existing studies. It is also demonstrated how our proposed model differs from previous works.

3. Proposed method

The proposed work consists of three phases: pre-processing, data embedding, and data extracting. Our Initial phase of pre-processing is explained in Section 3.1. Data embedding is present in Section 3.2 and finally Section 3.3 goes over our extraction phase. Figs. 1 and 2 depict the overall proposed method.

3.1. Pre-processing phase

As our target is to implant more bits in edge pixels than the non-edges, both the data hider and the data extractor should detect and identify the same set of edge pixels. To do that equally, a homogeneous field is required where both the data hider and data extractor can detect the same set of edge pixels. Previous works commonly applied their edge detectors in that homogeneous field. But, in that stage, our target is to apply a predictor on that homogeneous field and, thereafter, to compute the prediction errors. We would then want to compute edge pixels with the help of that prediction error space. These pre-processing tasks are shown in blocks of the first four levels of Fig. 1 Encoder.

3.1.1. Generating homogeneous field

Before starting that discussion, let the taken cover image is C and an instance of it is I. We first clear n-bits of LSBs from every pixel of I. To explain the LSB clearing method, consider a pixel value at (i, j) location of I, i.e., $I(i, j)$, is 175. The binary conversion of that pixel value is 01001011. Then, clearing 3 bits of LSBs from 01001011 will yield 01001000. In decimal, it will be 72. We generalize that clearing of n-bits of LSBs from each pixel by Eq. (9).

$$I(i, j) = I(i, j) - \Psi(I(i, j), 2^n); \tag{9}$$

where function Ψ returns the remainder value when one divides $I(i, j)$ by 2^n.

3.1.2. Generating prediction error space

Let the height and width of image I be h and w, respectively. Then, the predicted values of four corner pixels are computed by Eq. (10).

$$\begin{cases} p(1,1) = \frac{I(1,2)+I(2,1)}{2} \\ p(1,w) = \frac{I(1,w-1)+I(2,w)}{2} \\ p(h,1) = \frac{I(h-1,1)+I(h,2)}{2} \\ p(h,w) = \frac{I(h-1,w)+I(h,w-1)}{2} \end{cases} \tag{10}$$

Similar way, the other pixels in the first row, last row, first column, and last column are calculated by Eq. (11).

$$\begin{cases} p(1,j) = \frac{I(1,j-1)+I(2,j)+I(1,j+1)}{3} \\ p(h,j) = \frac{I(h,j-1)+I(h-1,j)+I(h,j+1)}{3} \\ p(i,1) = \frac{I(i-1,1)+I(i,2)+I(i+1,1)}{3} \\ p(i,w) = \frac{I(i-1,w)+I(i,w-1)+I(i+1,w)}{3} \end{cases} \tag{11}$$

In the same way, we compute all other middle pixels by Eq. (12).

$$p(i,j) = \frac{I(i-1,j)+I(i,j-1)+I(i+1,j)+I(i,j+1)}{4} \tag{12}$$

Thus, we compute all predicted values. Finally, the prediction errors and the absolute values of the prediction errors are calculated by Eqs. (13) and (14), respectively.

$$pE(i,j) = I(i,j) - p(i,j) \tag{13}$$

$$pE^a(i,j) = |pE(i,j)| \tag{14}$$

where $1 \le i \le h$, $1 \le j \le w$ and $|a|$ stands for absolute value of a.

3.1.3. Edge image generation

We have applied m-number of 'edge detection operators', e.g., canny, sobel, fuzzy, Robert, Prewitt, log, etc., on pE^a to measure edge pixels, separately. We have generated the edge image by Eq. (15).

$$eI(i) = f(pE^a, \Omega) \tag{15}$$

where Ω is one of the m edge detection operators, i.e., $\Omega \in \{Canny, Sobel, Log, Fuzzy, Robert, Prewitt, etc.\}$, $1 \le i \le m$ and f returns the edge image eI from pE^a for a specific edge detector Ω. Each edge image is a binary image. For each pixel, the edge image holds a 0 or 1. A 1 in edge image means the corresponding pixel (indeed, absolute error) of image pE^a is in the detected edge. We consider that the edges in pE^a are the edges of I. The experiment reveals that the number of edge pixels in pE^a is more than that in I for the same edge detector. Hence, the application of an edge detector in pE^a will provide us with more edge

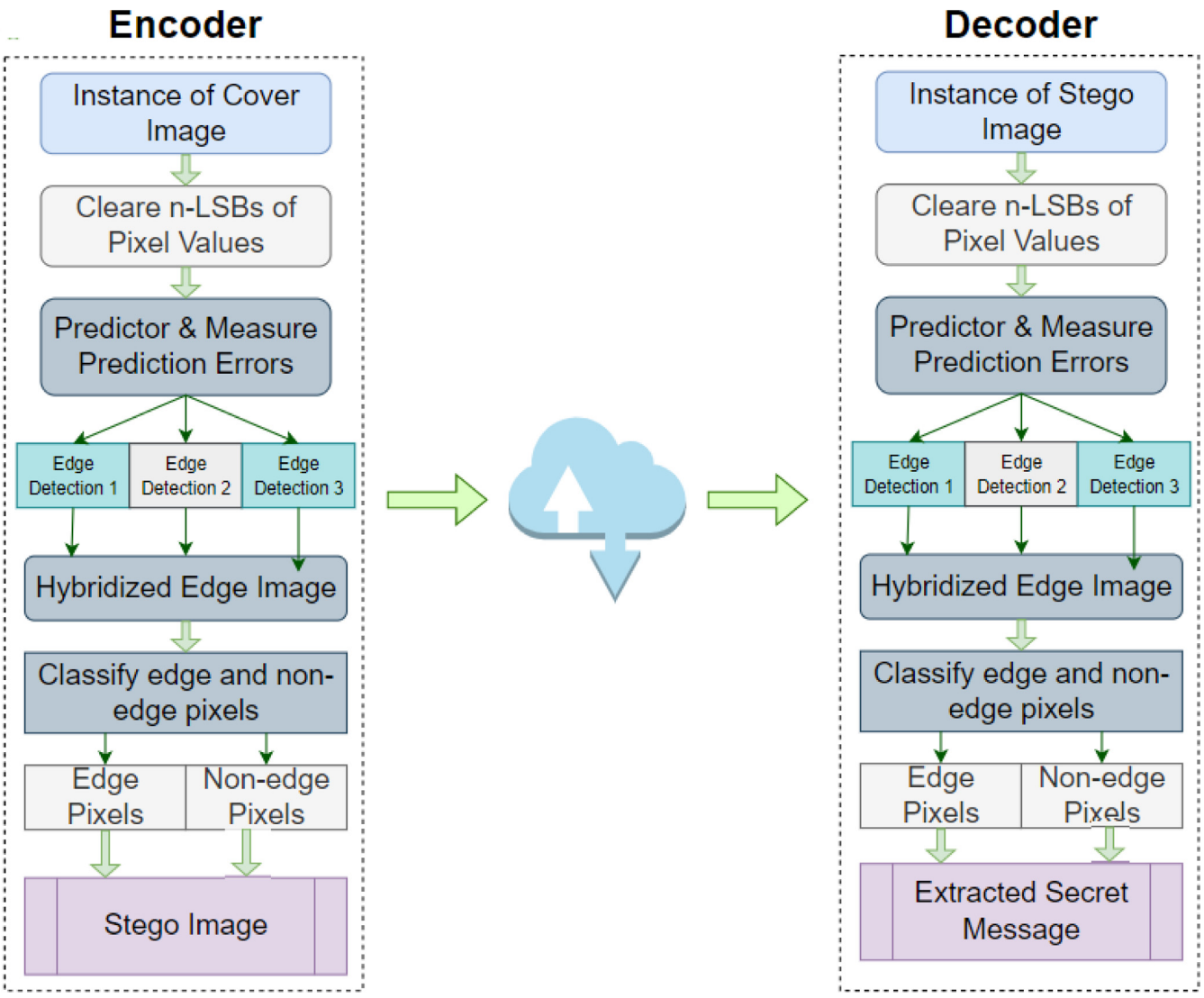

Fig. 1. The Encoder-Decoder architectures of the Proposed Method.

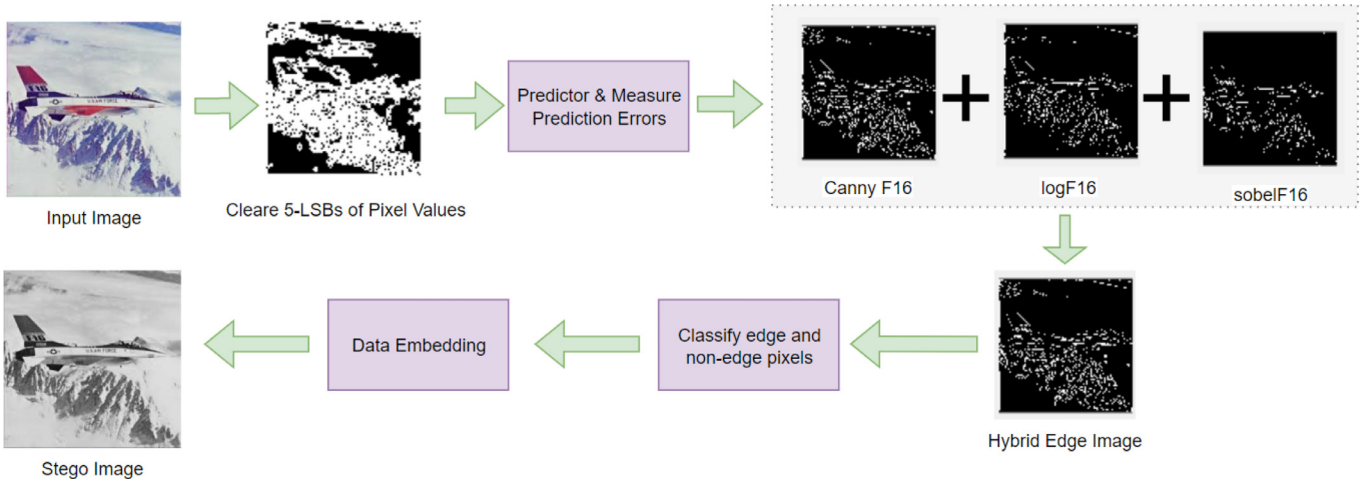

Fig. 2. The top-level overview of the Proposed Method.

pixels in I. Our objective is to enhance the embedding capacity of an edge detection-based scheme. Therefore, such an attempt will lead us to our goal. To improve further, we have combined the detected edge results. To do that, we have applied logical OR operations among the edge images. The OR image, i.e., resultant image $rI(i,j)$, is computed by Eq. (16).

$$rI(i,j) = eI(1,i,j) \vee eI(2,i,j) \vee \ldots \vee eI(m,i,j) \tag{16}$$

where $1 \le i \le h, 1 \le j \le w$ and $\vee$ stands for logical OR operator. This way, we have generated the resultant edge image from prediction error space by hybridizing edge detectors.

3.2. Data implantation phase

Now, it is the turn to embed secrets in image I. The whole data hiding process is depicted in Fig. 1 Encoder. The data-hiding steps are as follows:

- A module is developed to classify edge and non-edge pixels and their location in I. That classification is done using the help of the resultant edge image rI. The Eq. (17) is used to do that.

$$[eP, ePP, neP, nePP] = F(I, rI) \tag{17}$$

where F returns edge pixels eP, their positions ePP, non-edge pixels neP and their positions $nePP$ in I. The function F performs the calculation of these four return values by the following module of F.

Function $F(I, rI)$
Compute the size of image I. Let it is (h, w)
$[eP, ePP] = G_e(I, rI, h, w)$
$crI = (rI - 1) \times (-1)$
$[neP, nePP] = G_e(I, crI, h, w)$
return $[eP, ePP, neP, nePP]$

where G_e is defined below.

Function $G_e(A, B, h, w)$
$k = 0$
for $i = 1$ to h
for $j = 1$ to w
if $B(i,j) == 1$
$R_1(k) = A(i,j)$
$R_2(k,1) = i, R_2(k,2) = j$
return R_1, R_2

- Next, we implant x bits and y bits of secrets in each edge and non-edge pixel, respectively, of the cover image by the LSB substitution method. Let x-bits of information is b_x and y-bits of information is b_y. In that, the substitution task is performed by Eq. (18)

$$\begin{cases} S(s,t) = I(s,t) + \Phi(b_x) \\ S(u,v) = I(u,v) + \Phi(b_y) \end{cases} \tag{18}$$

where $\Phi(b_x)$ stands for decimal conversion of binary b_x, $s = ePP(i,1), t = ePP(i,2)$, $u = nePP(j,1), v = nePP(j,2)$ and $1 \le i \le No\_Of\_Edge\_Pixels, 1 \le j \le No\_Of\_nonEdge\_Pixels$. Here, b_x will be different for each of the s and t. The same is true for b_y. This means that, each time a different b_x and b_y of secret will be implanted.

That stego image S is then sent to a receiver end. The receiver end next extracts the implanted secrets from S.

3.3. Extraction phase

The extraction phase undergoes necessary pre-processing tasks. The extraction phase is depicted in Fig. 1 Decoder. Like the sender, the receiver copies the stego image S to I. It then clears n bits of LSBs from I by Eq. (9). Consider, that n-LSB cleared image is also I. The scheme then applies the same predictor to I to predict its pixel values. That prediction of pixel values is done by Eqs. (10) to (12). Again, Eqs. (13) and (14) compute the prediction errors and their absolute values, respectively. The absolute values of prediction errors are pE^a. Using Eq. (15) we have computed edge image $eI(i)$ from pE^a for different edge detectors Ω. Combining all edge images by Eq. (16), we form the resultant edge image rI. We have separated the edge pixels eP and their corresponding positions ePP in I by Eq. (17). The same Eq. (17) helps us in finding non-edge pixels neP and their positions $nePP$ in I. Next from each of the edge-located pixels, i.e., from (s,t), we have measured d_x, where $d_x = S(s,t) - I(s,t)$. Similar way, from each of the non-edge located pixels, we have computed d_y by $d_y = S(u,v) - I(u,v)$. Here, s, t, u, v, i, and j are defined in the immediate previous subsection. Next, we have extracted the binaries of the secret by Eq. (19).

$$\begin{cases} b_x = \Phi(d_x) \\ b_y = \Phi(d_y) \end{cases} \tag{19}$$

where $\Phi^(d_x)$ means binary conversion of decimal value d_x and $\Phi^(d_y)$ means binary conversion of decimal value d_y.

Fig. 1 Decoder represents the overall extraction phase.

4. Result analysis

This Section is divided into several sub-sections. In Section 4.1 we go over the experimental setup with which our study is carried out. Section 4.4 discusses the mathematical representation of feature values. Later in Section 4.5 we analyze the complexity. Section 4.2 reveals our experimental results. Finally, Section 4.3 provides a clear discussion regarding our findings.

We have investigated and compared the performance of the proposed scheme with the works of Bai et al. [24], Setiadi [25], Sultana et al. [32] and Rasol et al. [34]. We first selected images for the experiment, set up our experiment, and then analyzed the results.

4.1. Experimental setup

We worked on MATLAB's edition R(2017a) on Windows 7. The configuration of the laptop was comprised of an Intel (R) Core (TM) i5-8500T CPU@ 2.10 GHz 2.11 GHz processor and RAM of 8.00 GB. We first collected 10 commonly used images, as shown in Fig. 3, as a standard image dataset. We conducted all primary experiments on that standard image dataset. To test our scheme in a large image dataset, we used the BOSS dataset [33]. The BOSS dataset consisted of 499 images. We resized the images to 512×512 and converted the color to grayscale to fit our program.

We developed two different programs for each of the proposed methods, Bai et al., Setiadi D. R. I. M., Sultana et al. and Rasol et al. where one is for data implantation and the other is for retrieving the implanted secrets from stegos. According to the algorithm, we cleared n bits of LSBs from the cover images. We then verified the schemes by implanting different numbers of bits in edge and non-edge pixels, however, these are no more than n bits in any way. The performance of the schemes is verified by several feature values, such as edge pixel generation capability, embedding payload, peak signal-to-noise ratio (PSNR), structural similarity index matrix (SSIM), standard deviation, correlation coefficient, entropy, cosine similarity, pixel difference histogram, and chi-square text, etc.

4.2. Experimental results

In order to distinguish between edge and non-edge pixels in the experiment, we initially employed Canny, Sobel, and Log edge detectors in one, three, and five LSBs cleared images. When given an input image, the Canny, Sobel, and Log-based edge detector functions of MATLAB return an edge image. Binary images are used for edges. Utilizing 10 input images as a starting point, Table 2 depicts the edge images that were generated. It is already mentioned that the embedding rules implant x bits of information in edge pixels and y bits of information in

Table 2
Edge images generated from ten cover images. The images were formed for Canny, Sobel, and Log edge detectors both from original images ($n = 0$) and 5-LSBs cleared images ($n = 5$).

Image	Edge images for n=0			Edge images for n=5		
	Canny	Sobel	Log	Canny	Sobel	Log
Baboon				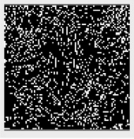	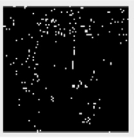	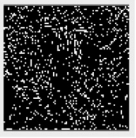
Basket			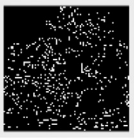			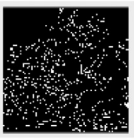
Boat				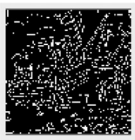		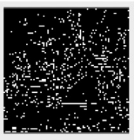
Barbara			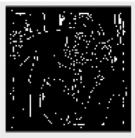			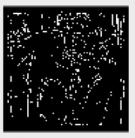
F16	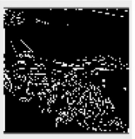			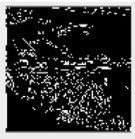	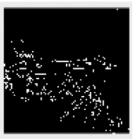	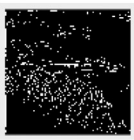
Lena			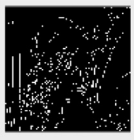	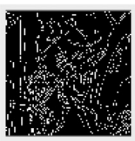		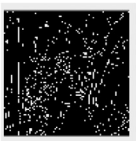
Living room	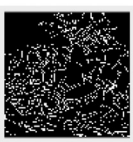		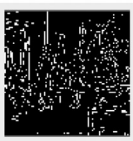	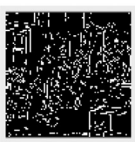		
Pepper						
Walk bridge						
Wheel						

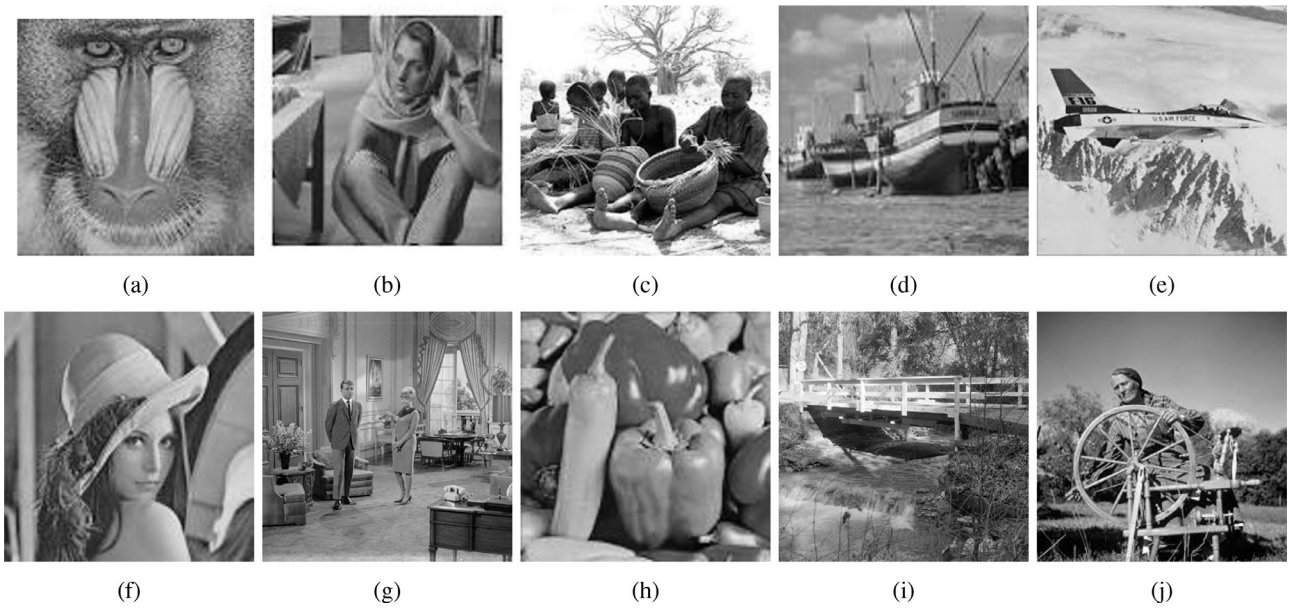

Fig. 3. Cover images for the experiment (**a**) Baboon, (**b**) Barbara, (**c**) Basket, (**d**) Boat, (**e**) F16, (**f**) Lena, (**g**) Livingroom, (**h**) Peppers, (**i**) Walkbridge, (**j**) Wheel.

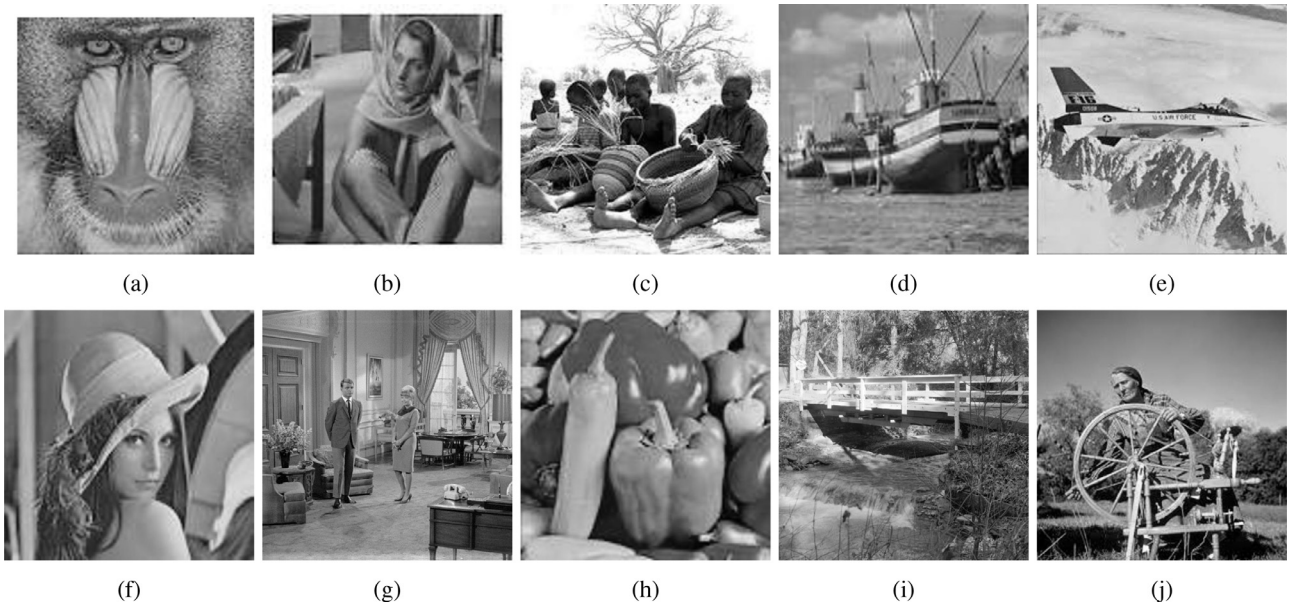

Fig. 4. Stego images for the corresponding cover images: (**a**) Baboon, (**b**) Barbara, (**c**) Basket, (**d**) Boat, (**e**) F16, (**f**) Lena, (**g**) Livingroom, (**h**) Peppers, (**i**) Walkbridge, (**j**) Wheel.

non-edge pixels. In all following discussions, we will represent that as a tuple (x, y). As $x > y$, an attempt of increasing the number of edge pixels will certainly boost the yielded embedding capacity. We did it by detecting edges in prediction error space. The justification is shown in Figs. 3 and 4. Table 3 also summarises the number of edge pixels that were found in ten sample images by different methods. Table 3 provided statistics collected from 5-LSBs cleared images.

We analyzed all the proposed and competing schemes to check their quantitative ability in hiding data. For that, all the schemes were experimented with for different values of (x, y). Here Tables 5 and 6 represent the payload results for $(x, y) \in \{(2, 1), (3, 1), (3, 2), (4, 1), (4, 2), (4, 3)\}$. There, a list of how much data can be hidden by a scheme for each of the different values of (x, y) is published. We analyzed the performance in the embedding capacity as well. Embedding capacity is graphically shown in Fig. 7 for $(x, y) = (4, 1)$. The same result is depicted in Fig. 8 for 499 images of the BOSS dataset.

We also analyzed the visual quality and structural originality of stego images. Visual quality is measured by PSNR values. Payload per losses of PSNR is sketched in Fig. 9. The structural similarity index value, SSIM, for every (x, y) are listed in Tables 7 and 8.

4.3. Discussions on results

The primary objective of this research is to strengthen the data-hiding ability of our scheme in terms of implanted data amount. As we worked on edge detection-based data embedment arena and the proposed scheme implanted more bits in edge pixels than the non-edge ones, we gave emphasis to increasing the number of edge pixels. For this, we applied the edge detector algorithms in prediction error space. Experiments have shown that this method is quite effective. The results of Fig. 5 is a snap-shoot of our experiment that is done on Lena's image. The figure is annotated with obtained edge pixels. Compared to

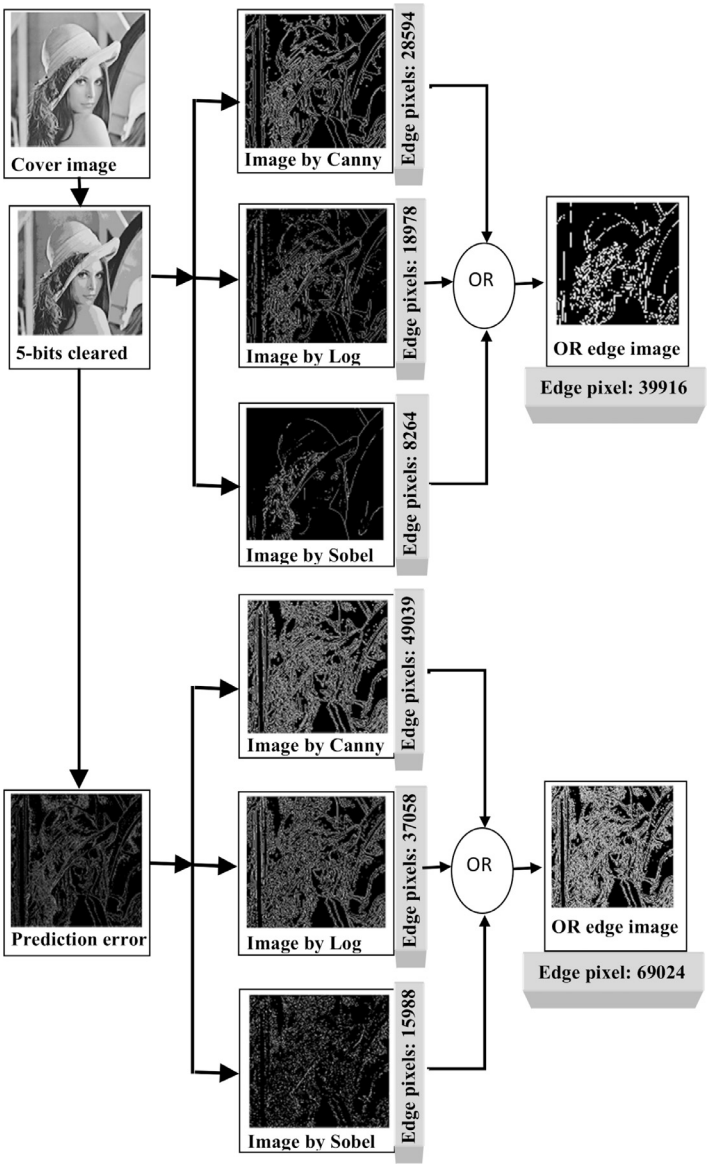

Fig. 5. A scene of how the edge detectors perform in prediction error space in detecting edge. The figure shows that each edge detector detects a large number of edge pixels in the prediction error space than in the image domain. Since our target is to increase the number of Edge pixels, this figure proves that the application of an edge detector in prediction error space has been successful.

Table 3
Statistics of Edge pixels for $n = 5$.

Image	Methods				
512×512	Proposed	Bai	Setiadi	Sultana	Rasol
F16	120,261	24,966	69,625	17,640	23,416
babon	176,798	38,383	100,727	4718	34,566
basket	159,679	31,560	86,141	21,975	31,223
boat	138,274	26,991	82,727	32,813	24,326
brbra	140,756	26,941	74,693	6272	18,521
lena	126,397	24,884	75,604	27,664	21,032
livingroom	186,518	35,543	102,571	27,118	36,722
pepper	136,479	25,860	80,497	31,724	19,259
walkbridge	199,069	45,563	123,388	24,133	44,923
wheel	142,915	27,745	75,688	21,585	29,419

state-of-art, that number is about double in our scheme. For ten images of the standard dataset, the results are shown in detail in Fig. 5 and Table 3. Table 3 states the results for $n = 5$, where Fig. 5 depicts the same for $n = 1$, $n = 3$ and $n = 5$. Corresponding embedding capacities are depicted in 6. The results of Figs. 5 and 6 and Table 3 confirm that all edge detectors recognize more contents as edge contents in prediction error space.

After justifying that truth, we implanted secrets in edge and non-edge pixels at a rate of (x, y). The embedding capacity is depicted in Fig. 7 for ten sample images. The figure states that the proposed scheme enhances the embedding capacity by about Bai 80% of et al. [24], 50% of Setiadi [25], 90% of Sultana et al. [32] and 70% of Rasol et al. [34]. To justify the performance of the proposed scheme, we experimented on 499 images of the BOSS dataset as well. The experiments said the same fact. Those results are summarised in Fig. 9 In all the images, the proposed scheme provides dominating results over the other competing schemes. However, those depicted results were obtained for $(x, y) = (4, 1)$ only. Table 4 represents the results for all combinations of (x, y), e.g., $(x, y) \in \{(2, 1), (3, 1), (3, 2), (4, 1), (4, 2), (4, 3)\}$. Additionally, this table also explains that the proposed scheme offers much more payloads than the alternatives. That the proposed scheme considerably enhances the embedding capacity is therefore validated.

When a scheme implants its secrets in an image, obviously, it destroys the visual quality of that image. We measured the number of bits that were implanted in an image per one dB of $PSNR$ loss. The measurement is illustrated graphically in Fig. 9. It is easy to see from the diagram that the proposed scheme implants a satisfactory amount of data as opposed to one dB PSNR loss, and it is higher than the competing schemes. Again, the results of SSIM are figured out in Table 5 for

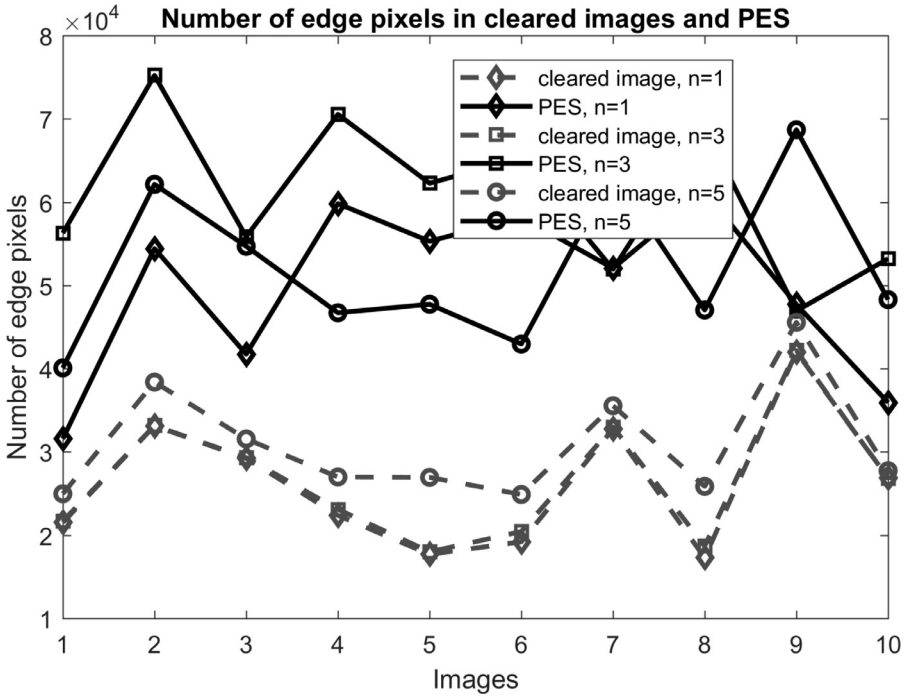

Fig. 6. Number of edge pixels in image and prediction error space (PES). After clearing 1-bit LSB, we computed edge pixels that were detected by Canny. A similar approach was done for 3-bit and 5-bit LSB-cleared images. These are represented in the figure by solid lines and diamond, square, and circle markers, respectively. The same was done by applying our predictor and then employing Canny in PES. These results are presented by dash lines and diamond, square, and circle markers, respectively. The figure states that Canny well performs in all PES-based experiments.

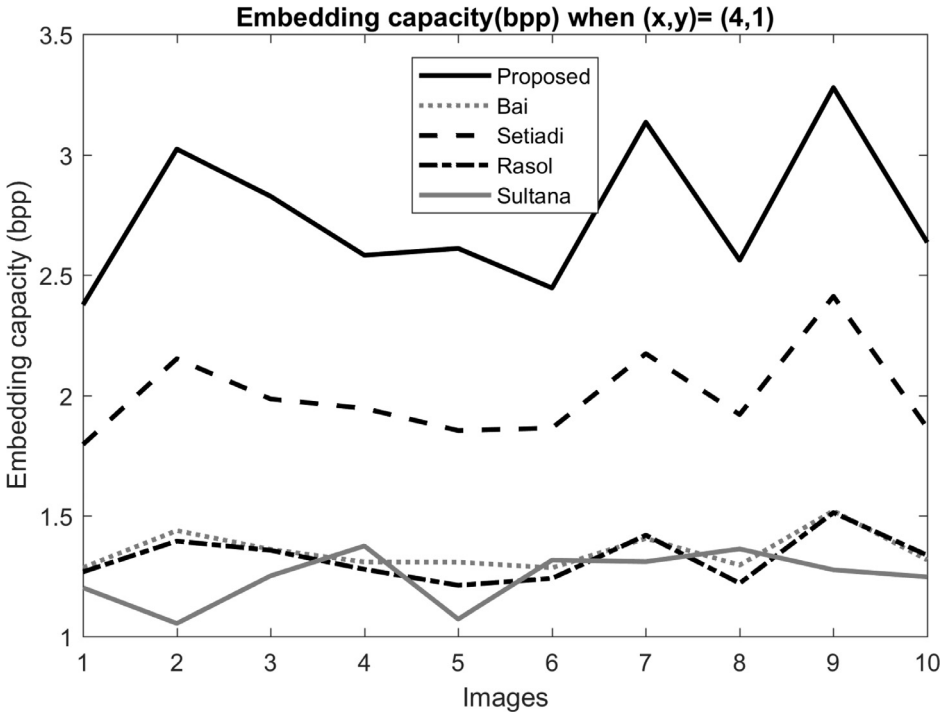

Fig. 7. Comparison of embedding rate. This figure is generated by embedding at (x,y)=(4,1). The figure states that the proposed scheme yields embedding capacity at a dominating rate which is about 50% higher than Setiadi, 70% higher than Rasol et al., 80% higher than Bai at al. and 90% higher than Sultana et al.

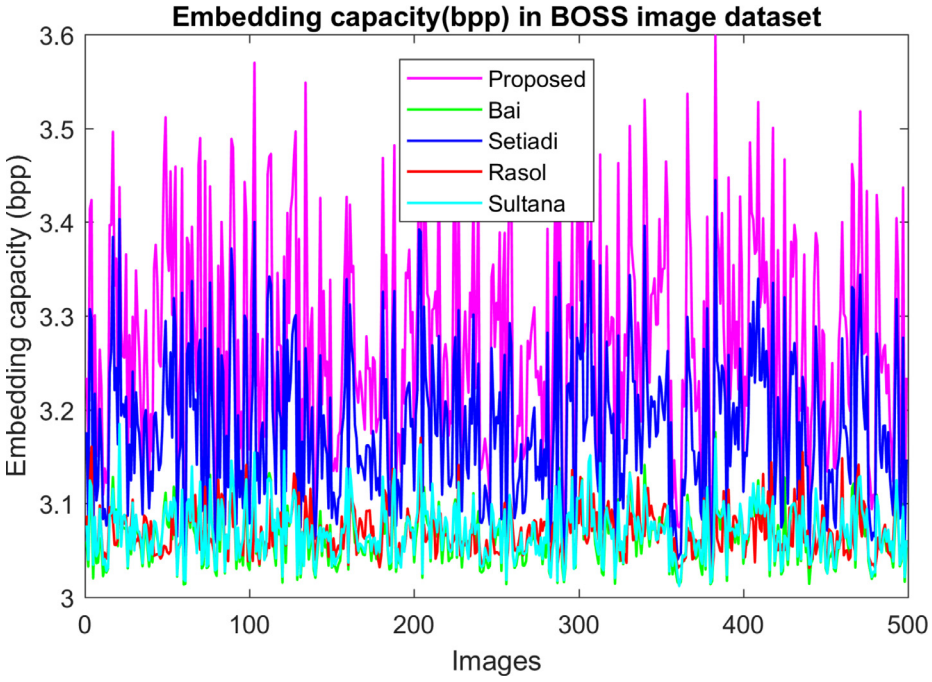

Fig. 8. Performance comparison of the proposed scheme with Bai, Setiadi, Sultana, and Rasol in terms of capacity in the BOSS image dataset. That experiments were done to justify the proposed scheme in a large image dataset. The figure states that our proposal is unbeaten in producing a larger embedding capacity.

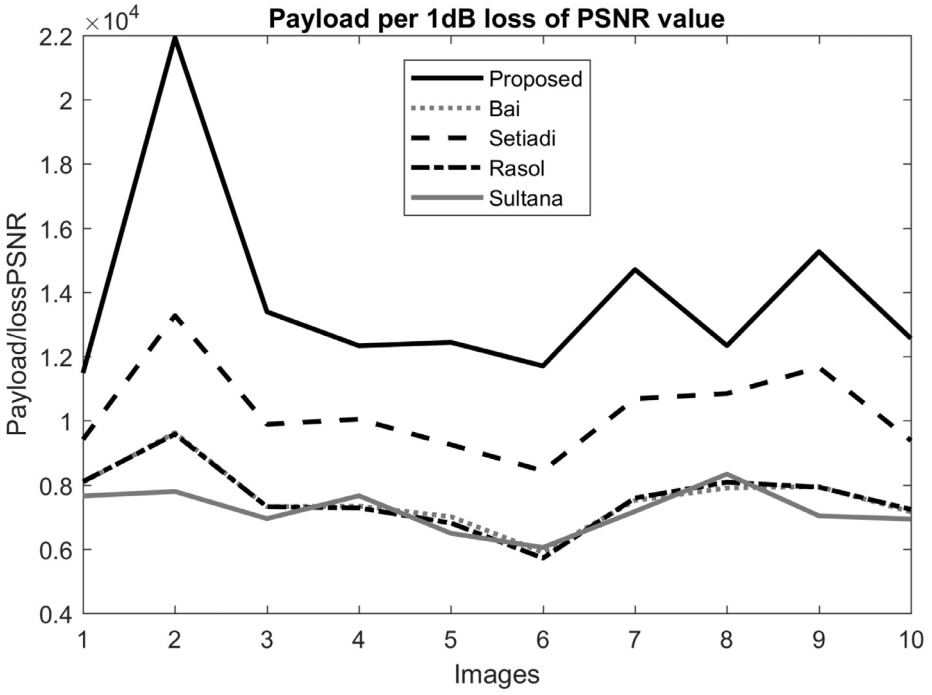

Fig. 9. Number of embedded bits per 1dB loss of PSNR. Regarding that per 1dB loss of PSNR, the proposed scheme noticeably dominates the other competing schemes.

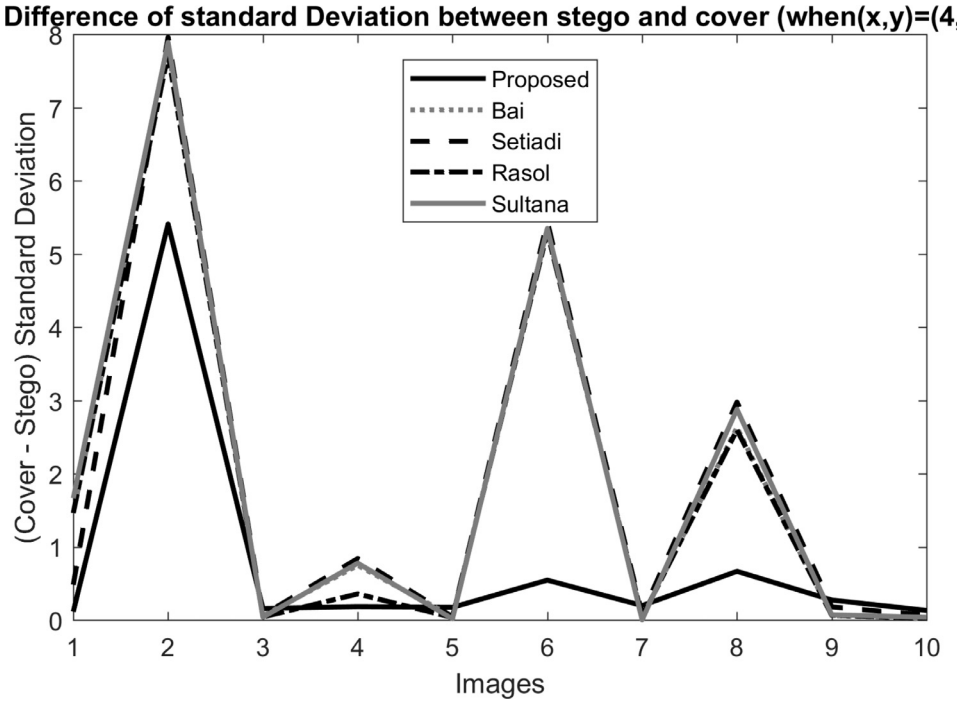

Fig. 10. Difference of standard Deviations of cover and stego images. The figure states that the differences are very small, close to each other. The proposed method is closer to zero.

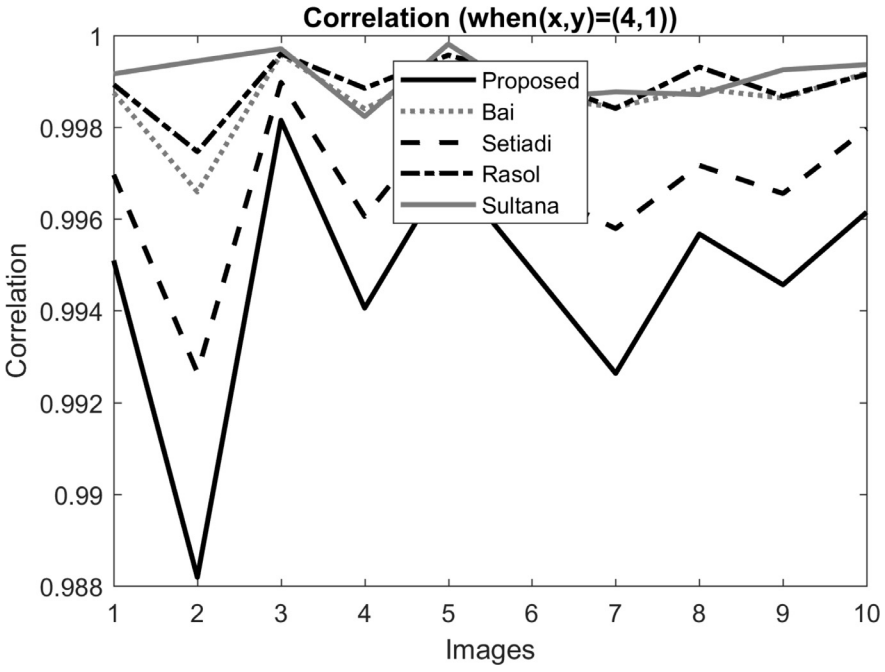

Fig. 11. Correlation coefficients. All the schemes present higher correlations.

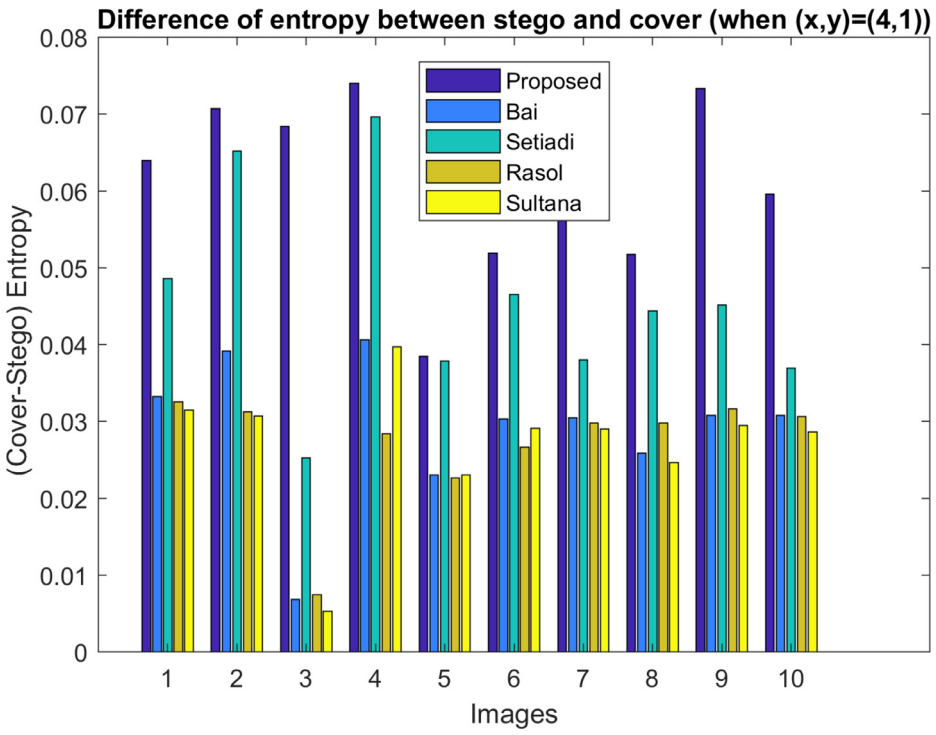

Fig. 12. Difference of entropy between cover and stego. The differences are very small and insignificant to mention.

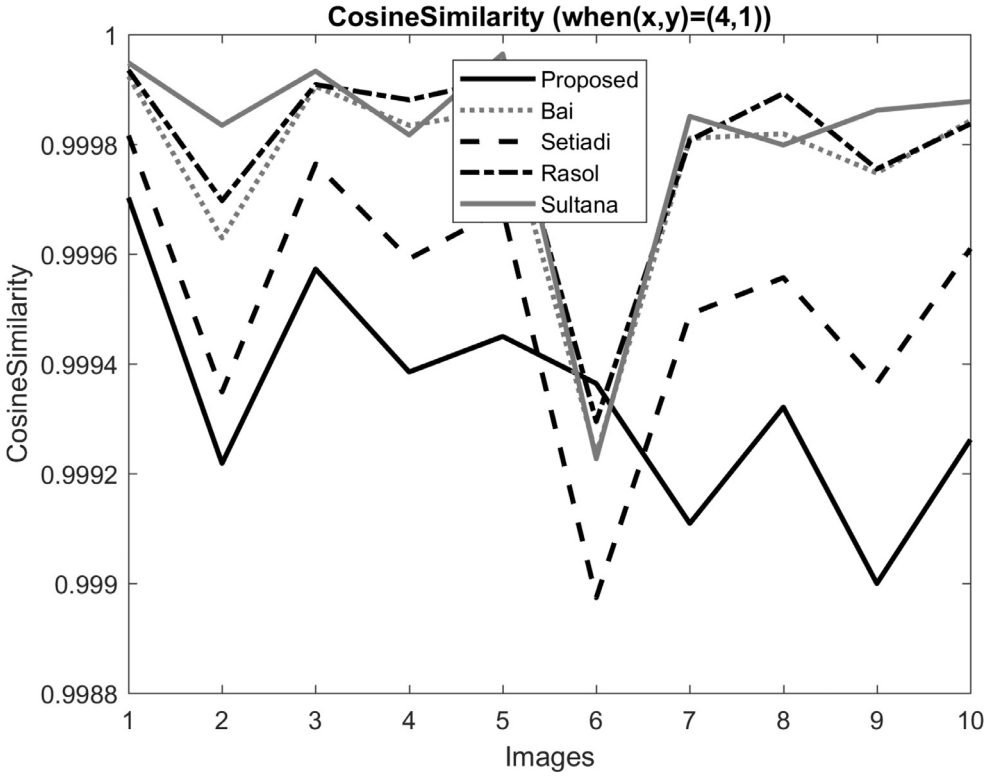

Fig. 13. Cosine similarity values. Measured cosine similarity values are very high in all the images.

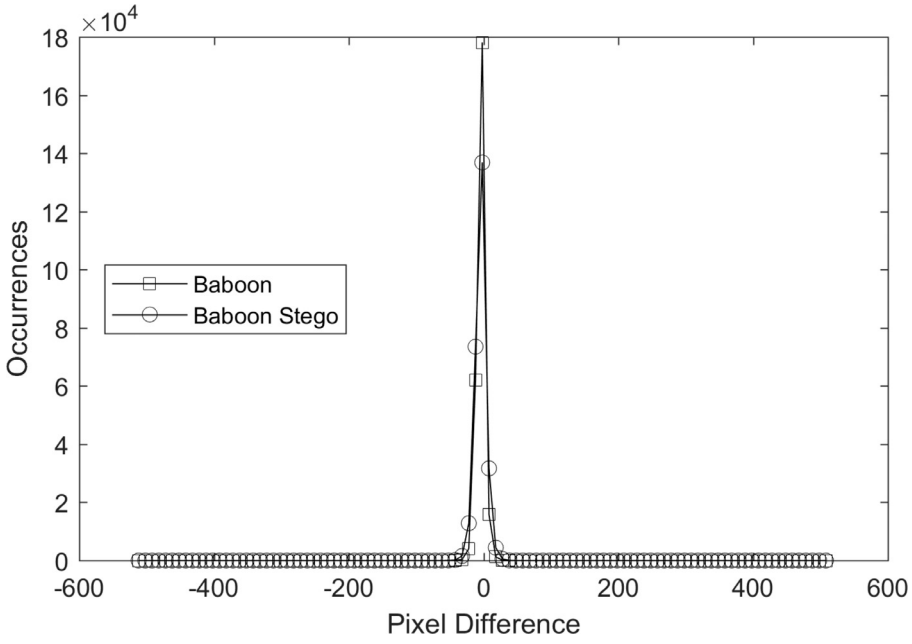

Fig. 14. Pixel Difference Histogram of Baboon.

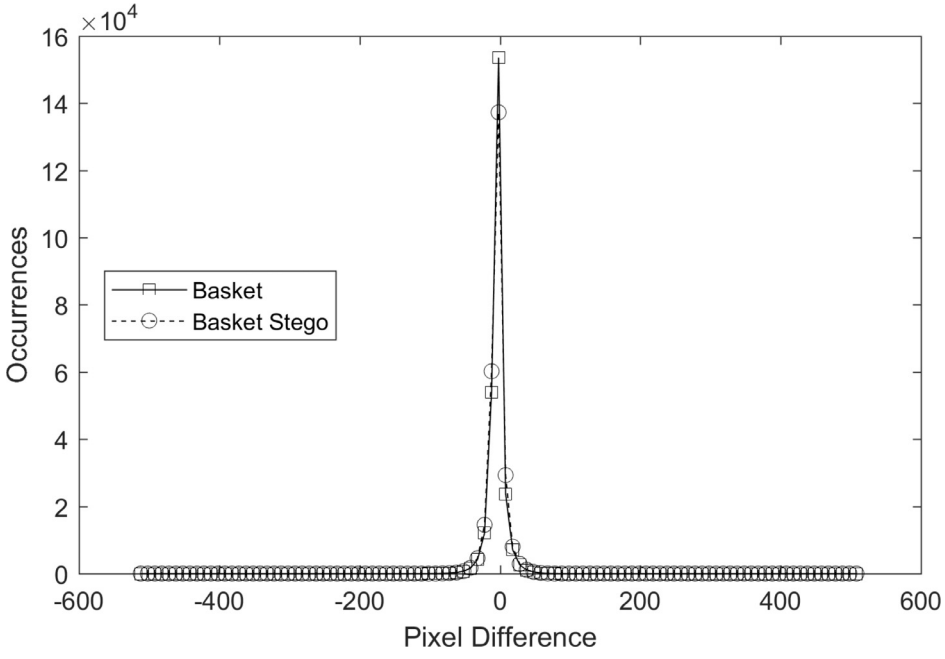

Fig. 15. Pixel Difference Histogram of Basket.

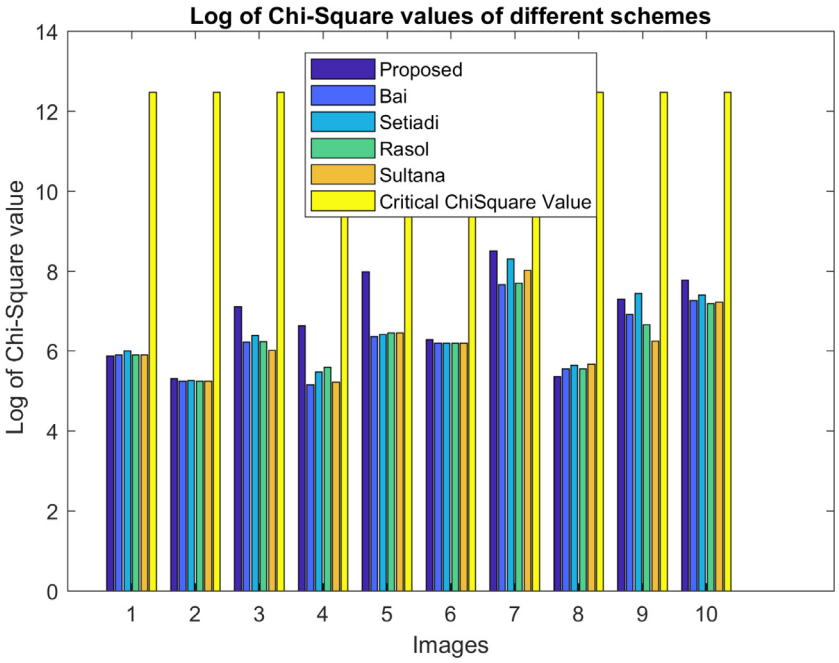

Fig. 16. Comparison of chi-square values among the schemes in the logarithmic scale.

Table 4
Execution time per image (in seconds).

Image	Methods				
512 × 512	Proposed	Bai	Setiadi	Sultana	Rasol
F16	14.40	13.37	13.90	13.34	13.52
babon	14.92	13.43	14.26	13.15	13.64
basket	14.75	13.42	14.03	13.46	13.53
boat	14.53	13.69	13.95	13.62	13.45
brbra	14.39	13.31	13.92	13.08	13.35
lena	14.36	13.30	13.91	13.56	13.39
livingroom	15.14	13.49	14.18	13.45	13.58
pepper	14.41	13.33	14.00	13.57	13.41
walkbridge	15.29	13.64	14.49	13.51	13.78
wheel	14.54	13.24	13.94	13.57	13.56

all the stated combinations of (x, y). Depending on the distortion rate SSIM value ranges from 0 to 1. A higher value of SSIM signifies better originality of the image. The table confirms that the SSIM values of all the schemes are both high and very close to each other. Though these schemes randomly dictate one another, there is nothing significant to mention about the level of dictation. Thus, we can conclude that the proposed schemes do not destroy the quality of the image at any significant level, and are even higher than the others.

4.4. Mathematical representation of feature values

Payload is the total number of implanted bits in the cover image. Let the number of edge and non-edge pixels in a cover image be epT and npT, respectively. Then the maximum achievable payload PL is defined by Eq. (20).

$$PL = epT \times x + npT \times y \tag{20}$$

Sometimes, capacity is also measured to have a closer look at the performance of a scheme. Capacity means the number of implanted bits per pixel. Embedding capacity, EC, is measured by Eq. (21)

$$EC = \frac{p}{h \times w} \tag{21}$$

Where h and w are the image height and width.

While hiding data, maintaining image quality is a challenging issue. PSNR and SSIM are two commonly used image distortion measurement parameters. PSNR is measured by Eq. (22).

$$PSNR = 10 \log_{10} \frac{255^2}{MSE} \tag{22}$$

Where,

$$MSE = \frac{1}{h * w} \sum_{i=1}^{w} \sum_{j=1}^{h} (S_{i,j} - Ci, j)^2;$$

here, S is the stego image and C is the original cover image.

We expect to have our $PSNR$ value at 100dB. That $PSNR$ is, indeed, achievable for two identical images only. However, the stego image is a tempered image. Hence, the value of $PSNR$ will deteriorate. The amount of loss in $PSNR$ value, let $lossPSNR$, is measured by (23).

$$lossPSNR = (100 - PSNR)dB \tag{23}$$

Again, SSIM is calculated by Eq. (24).

$$SSIM = \frac{(2\mu_c\mu_s + C_1)(2\sigma_{cs} + C_2)}{(\mu_c^2 + \mu_s^2 + C_1)(\sigma_c^2 + \sigma_s^2 + C_2)} \tag{24}$$

In Eq. (24), μ_c and σ_c are the mean and variance of pixel values in the cover image. Likewise cover, μ_s and σ_s are the same for the stego image. Again, σ_{cs} is the co-variance between the cover and stego image. C_1 and C_2 are two constants. In experiment, we set $C_1 = 0.0001$ and $C_2 = 0.0009$

There are many methods of analyzing the security of a scheme. Very simple but common ones are entropy measurement, analyzing correlation among the pixels, and checking the cosine similarity between the cover and stego image. The entropy is measured by Eq. (25).

$$H = -\sum_{k} p_k \log_2(p_k) \tag{25}$$

where, p_k is the probability associated with gray value k and $1 \le k \le 255$.

In our experiment, we used the population correlation coefficient. Populations were measured from the pixel histogram. Population correlation is defined by Eq. (26).

$$\rho_{cs} = \frac{\sigma_{cs}}{\sigma_c \sigma_s} \tag{26}$$

where σ_c and σ_s are population standard deviations in cover C and stego S. Again, σ_{cs} is the co-variance between the cover and stego image.

Table 5
Comparison of the payload of the proposed scheme with its competing methods.

Image	Methods														
	(x,y)=(2,1)					(x,y)=(3,1)					(x,y)=(3,2)				
	Proposed	Bai	Setiadi	Sultana	Rasol	Proposed	Bai	Setiadi	Sultana	Rasol	Proposed	Bai	Setiadi	Sultana	Rasol
F16.jpg	382,405	287,110	331,769	279,784	285,560	502,666	312,076	401,394	297,424	308,976	644,549	549,254	593,913	541,928	547,704
babon.jpg	438,942	300,527	362,871	266,862	296,710	615,740	338,910	463,598	271,580	331,276	701,086	562,671	625,015	529,006	558,854
basket.jpg	421,823	293,704	348,285	284,119	293,367	581,502	325,264	434,426	306,094	324,590	683,967	555,848	610,429	546,263	555,511
boat.jpg	400,418	289,135	344,871	294,957	286,470	538,692	316,126	427,598	327,770	310,796	662,562	551,279	607,015	557,101	548,614
brbra.jpg	402,900	289,085	336,837	268,416	280,665	543,656	316,026	411,530	274,688	299,186	665,044	551,229	598,981	530,560	542,809
lena.jpg	388,541	287,028	337,748	289,808	283,176	514,938	311,912	413,352	317,472	304,208	650,685	549,172	599,892	551,952	545,320
livingroom.jpg	448,662	297,687	364,715	289,262	298,866	635,180	333,230	467,286	316,380	335,588	710,806	559,831	626,859	551,406	561,010
pepper.jpg	398,623	288,004	342,641	293,868	281,403	535,102	313,864	423,138	325,592	300,662	660,767	550,148	604,785	556,012	543,547
walkbridge.jpg	461,213	307,707	385,532	286,277	307,067	660,282	353,270	508,920	310,410	351,990	723,357	569,851	647,676	548,421	569,211
wheel.jpg	405,059	289,889	337,832	283,729	291,563	547,974	317,634	413,520	305,314	320,982	667,203	552,033	599,976	545,873	553,707

Table 6
Comparison of the payload of the proposed scheme with its competing methods.

Image	Methods														
	(x,y)=(4,1)					(x,y)=(4,2)					(x,y)=(4,3)				
	Proposed	Bai	Setiadi	Sultana	Rasol	Proposed	Bai	Setiadi	Sultana	Rasol	Proposed	Bai	Setiadi	Sultana	Rasol
F16.jpg	622,927	337,042	471,019	315,064	332,392	764,810	574,220	663,538	559,568	571,120	906,693	811,398	856,057	804,072	809,848
babon.jpg	792,538	377,293	564,325	276,298	365,842	877,884	601,054	725,742	533,724	593,420	963,230	824,815	887,159	791,150	820,998
basket.jpg	741,181	356,824	520,567	328,069	355,813	843,646	587,408	696,570	568,238	586,734	946,111	817,992	872,573	808,407	817,655
boat.jpg	676,966	343,117	510,325	360,583	335,122	800,836	578,270	689,742	589,914	572,940	924,706	813,423	869,159	819,245	810,758
brbra.jpg	684,412	342,967	486,223	280,960	317,707	805,800	578,170	673,674	536,832	561,330	927,188	813,373	861,125	792,704	804,953
lena.jpg	641,335	336,796	488,956	345,136	325,240	777,082	574,056	675,496	579,616	566,352	912,829	811,316	862,036	814,096	807,464
livingroom.jpg	821,698	368,773	569,857	343,498	372,310	897,324	595,374	729,430	578,524	597,732	972,950	821,975	889,003	813,550	823,154
pepper.jpg	671,581	339,724	503,635	357,316	319,921	797,246	576,008	685,282	587,736	562,806	922,911	812,292	866,929	818,156	805,691
walkbridge.jpg	859,351	398,833	632,308	334,543	396,913	922,426	615,414	771,064	572,554	614,134	985,501	831,995	909,820	810,565	831,355
wheel.jpg	690,889	345,379	489,208	326,899	350,401	810,118	579,778	675,664	567,458	583,126	929,347	814,177	862,120	808,017	815,851

Table 7
Comparison of SSIM results of the proposed scheme with other competing schemes.

Image	Methods														
	(x,y)=(2,1)					(x,y)=(3,1)					(x,y)=(3,2)				
	Proposed	Bai	Setiadi	Sultana	Rasol	Proposed	Bai	Setiadi	Sultana	Rasol	Proposed	Bai	Setiadi	Sultana	Rasol
F16.jpg	0.989	0.993	0.992	0.994	0.993	0.973	0.990	0.984	0.993	0.992	0.960	0.973	0.969	0.976	0.974
babon.jpg	0.962	0.972	0.969	0.974	0.972	0.927	0.962	0.948	0.973	0.967	0.924	0.949	0.940	0.956	0.953
basket.jpg	0.994	0.997	0.996	0.997	0.997	0.980	0.995	0.991	0.997	0.995	0.974	0.986	0.983	0.988	0.986
boat.jpg	0.988	0.993	0.991	0.993	0.994	0.965	0.987	0.977	0.986	0.991	0.955	0.972	0.964	0.971	0.975
brbra.jpg	0.989	0.994	0.992	0.995	0.995	0.965	0.989	0.980	0.995	0.993	0.957	0.975	0.968	0.980	0.978
lena.jpg	0.982	0.987	0.984	0.987	0.988	0.960	0.980	0.969	0.980	0.984	0.946	0.962	0.954	0.962	0.966
livingroom.jpg	0.993	0.997	0.996	0.997	0.997	0.974	0.995	0.990	0.997	0.995	0.972	0.988	0.984	0.989	0.988
pepper.jpg	0.984	0.990	0.988	0.990	0.991	0.957	0.983	0.971	0.982	0.989	0.948	0.966	0.955	0.966	0.971
walkbridge.jpg	0.995	0.998	0.997	0.998	0.998	0.981	0.995	0.991	0.998	0.996	0.979	0.991	0.987	0.992	0.991
wheel.jpg	0.993	0.996	0.995	0.996	0.996	0.980	0.994	0.992	0.996	0.995	0.970	0.982	0.979	0.983	0.982

Table 8
Comparison of SSIM results of the proposed scheme with other competing schemes.

Image	Methods														
	(x,y)=(4,1)					(x,y)=(4,2)					(x,y)=(4,3)				
	Proposed	Bai	Setiadi	Sultana	Rasol	Proposed	Bai	Setiadi	Sultana	Rasol	Proposed	Bai	Setiadi	Sultana	Rasol
F16.jpg	0.925	0.975	0.955	0.992	0.984	0.914	0.959	0.942	0.975	0.968	0.879	0.911	0.895	0.922	0.917
babon.jpg	0.832	0.924	0.878	0.971	0.946	0.826	0.911	0.874	0.958	0.934	0.804	0.870	0.838	0.899	0.883
basket.jpg	0.933	0.987	0.972	0.995	0.989	0.928	0.978	0.964	0.986	0.981	0.909	0.947	0.937	0.953	0.950
boat.jpg	0.892	0.964	0.929	0.962	0.980	0.882	0.949	0.919	0.947	0.965	0.852	0.903	0.879	0.902	0.913
brbra.jpg	0.891	0.966	0.935	0.995	0.986	0.883	0.952	0.925	0.979	0.972	0.856	0.907	0.886	0.927	0.921
lena.jpg	0.890	0.953	0.915	0.954	0.973	0.879	0.936	0.901	0.937	0.955	0.847	0.886	0.860	0.886	0.899
livingroom.jpg	0.913	0.986	0.967	0.994	0.988	0.910	0.979	0.961	0.987	0.981	0.901	0.953	0.939	0.959	0.955
pepper.jpg	0.877	0.954	0.913	0.950	0.979	0.868	0.937	0.901	0.935	0.962	0.828	0.887	0.859	0.885	0.900
walkbridge.jpg	0.931	0.986	0.968	0.996	0.989	0.930	0.982	0.965	0.991	0.984	0.925	0.965	0.951	0.971	0.966
wheel.jpg	0.937	0.989	0.978	0.994	0.990	0.928	0.976	0.966	0.981	0.978	0.902	0.938	0.930	0.942	0.939

Equation (27) gives us the cosine similarity values.

$$f_{CosSim}(C,S) = cos(\theta) = \frac{\sum_{i=1}^{h}\sum_{j=1}^{w} C(i,j)S(i,j)}{\sqrt{\sum_{i=1}^{h}\sum_{j=1}^{w} C(i,j)}\sqrt{\sum_{i=1}^{h}\sum_{j=1}^{w} S(i,j)}} \quad (27)$$

where C and S are cover and stego images.

When they are the same, the function f_{CosSim} provides the highest value, which is 1. f_{CosSim}'s computed value depends on the tempering effect in image S. The more tempered in S, the smaller the value of f_{CosSim}.

4.5. Analyzing the complexity

We compare the time complexity of different schemes by analyzing their execution time and compared with existing studies and result is shown in Table 4. In terms of completion time author Bai's study outperformed every other study. On average author's proposed scheme require about 13.42 s [24]. Similar to Bai's study, Sultana and Rasol's proposed framework requires 13.43 and 13.52 s [32,34]. Setiadi's study on the other hand requires 14.06 s [25]. On average, our suggested method consumes 14.67 s per image. Even though it ends up taking a little bit longer, it exceeds all previous research and yields significantly superior outcomes as a consequence. Thus this difference of 0.5–1 s can be overlooked.

4.6. Security analysis

We statistically analyzed our scheme to check its robustness against various attacks. We first measured the standard deviation of pixel values from their mean, separately, in cover and stego images. Let the standard deviation in cover and stego image is σ_c and σ_s. Next, we calculated their difference by $\sigma_d = \sigma_c - \sigma_s$. Ideally, σ_d should be zero for a non-tempered image. That σ_d is drawn in Fig. 10 against different images. The results show that the proposed scheme produces smaller differences than the others and it is closer to zero. To verify further with similar statistics, we measured correlation coefficients $\rho_S C$ between the cover and stego image. $\rho_S C > 0$ means a positive correlation between cover and stego image and $\rho_S C$ signifies a perfect relationship when it reaches to 1. Similarly, a negative value of $\rho_S C$ indicates a negative relationship. $\rho_S C = 0$ stands for no relationship between two images. Results of $\rho_S C$ are depicted in Fig. 11. Though the proposed method shows a lower correlation value, its difference from others is insignificance. Rather, as with others, it represents a higher correlation between cover and stego.

We measured the entropy values H as well. We computed H both in cover and stego images. Next, we calculated their differences. That difference value is zero for two identical images. Results are plotted in Fig. 12. The figure shows that none of the results are greater than 0.08, i.e., these are very small and close to zero. We also computed cosine similarities between cover and stego images. That value is 1 for two identical images and 0 for two fully mismatched images. The results are demonstrated in Fig. 13. The figure illustrates that all the values are greater than 0.999, which is very high. Besides, the values in all the schemes are very close to each other, where, the maximum variation is o.0008, i.e., 0.9998-0.999.

Thus, it can be deduced from the results of these experiments that our method is strong enough to protect against attacks on implanted data.

We used statistical tools of pixel difference histogram (PDH) to identify the stego images. The PDH of the original images and corresponding stego images are shown in Figs. 14 and 15.

We also used another statistical tool of Chi-Square test for determining the difference between stego and cover images. This test is used to find out whether a difference between two images is due to chance or a relationship between them. The experimental result of the Chi-square test is shown in Fig. 16.

$$\chi_{DF}^{2} = \frac{\sum (S_i - C_i)^2}{C_i} \quad (28)$$

where DF is the degrees of freedom, C and S are cover and stego images. DF is calculated by (Fig. 16)

$$DF = (h-1) * (w-1) \tag{29}$$

Here h and w are the height and width of the cover and stego images (Tables 6–8).

5. Discussion

Using this research, it can secure both messages and communicating parties. No intruder can able to receive some beneficial information from the sending file during transmission. Besides Corporations government and law enforcement agencies can connect privately and communicate secretly.

Although this model has many advantages it also has some limitations. This model cannot work without edge detectors. This model consumes time when applying predictor and it is not a big matter. If a steganography approach generates someone to suspect the carrier medium, thus the model has been unsuccessful.

6. Conclusion

This research first time proposes the idea of grouping image pixels as edge and non-edge by applying an edge detector in its prediction error space. The research first generates a prediction error space from a cover image and then applies a desired predictor in that created error space. The locations of detected edge errors are mapped in the cover image to classify edge and non-edge pixels. That strategy, significantly, increases the number of edge pixels. As the edge detection-based embedding schemes implant more bits in edge pixels than non-edge pixels, the same rules then well perform in the proposed method. The experimental results deduce that the scheme does not compromise the visual or structural quality of the cover image more than the other competing schemes. Moreover, statistical analyses exhibit that the proposed scheme demonstrates stronger security against attacks. In the future, we hope to work on making the scheme reversible. At the same time, we would like to repeatedly embed an image with a back-and-forward strategy. In the back-and-forward strategy, we will increase the present values of pixels in the first cycle of data embedment and decrease the updated values in the second cycle of data embedment. Thus, we want to implant any length of the message in an image by managing its visual quality. In that case, managing the scheme's reversibility is a pre-requisition. We also would like to work with other media such as audio, video, and text. We will apply this model for forensic or other security purposes.

Availability of data and materials

We used data from "The Bank of Standardized Stimuli (BOSS), a New Set of 480 Normative Photos of Objects to Be Used as Visual Stimuli in Cognitive Research, Mathieu B. Brodeur, Emmanuelle Dionne-Dostie, Tina Montreuil, Martin Lepage" and various reliable sources (Internet).

CRediT authorship contribution statement

Habiba Sultana: Conceptualization, Methodology, Software. **A.H.M. Kamal:** Conceptualization, Methodology, Software. **Tasnim Sakib Apon:** Data curation, Writing – original draft.

Acknowledgments

The first author is a fellow of the ICT division of the Ministry of Post, Telecommunication, and Information Technology of the Government of Bangladesh. Therefore, we want to devote a thank to the concerned ministry, and at the same time, we would like to acknowledge that support.

References

[1] H. Al-Dmour, A. Al-Ani, A steganography embedding method based on edge identification and XOR coding, Expert Syst. Appl. 46 (2016) 293–306.
[2] H. Sultana, A study on steganography and steganalysis, Int. J. Sci. Eng. Res. 9 (12) (2018).
[3] H. Sultana, A.H.M. Kamal, An edge detection based reversible data hiding scheme, in: 2022 IEEE Delhi Section Conference (DELCON), IEEE, 2022.
[4] P.W. Adi, F.Z. Rahmanti, N.A. Abu, High quality image steganography on integer harr wavelet transform using modulus function, in: International Conference on Science in Information Technology (ICSITech), IEEE, 2015.
[5] H. Sultana, A.H.M. Kamal, M.M. Islam, Enhancing the robustness of visual degradation based HAM reversible data hiding, J. Comput. Sci. 12 (2) (2016) 88–97.
[6] A.H.M. Kamal, M.M. Islam, Enhancing embedding capacity and stego image quality by employing multi predictors, J. Inf. Secur. Appl. 32 (2017) 59–74.
[7] A.H.M. Kamal, M.M. Islam, Boosting up the data hiding rate through multi cycle embedment process, J. Vis. Commun. Image Represent. 40 (2016) 574–588.
[8] A.H.M. Kamal, M.M. Islam, Capacity improvement of reversible data hiding scheme through better prediction and double cycle embedding process, in: 2015 IEEE International Conference on Advanced Networks and Telecommuncations Systems (ANTS), IEEE, 2015.
[9] A.H.M. Kamal, M.M. Islam, An image distortion-based enhanced embedding scheme, Iran J. Comput. Sci. 1 (3) (2018) 175–186.
[10] A.H.M. Kamal, M.M. Islam, A prediction error based histogram association and mapping technique for data embedment, J. Inf. Secur. Appl. 48 (2019) 102368.
[11] A.H.M. Kamal, M.M. Islam, Z. Islam, An embedding technique for smartcard-supported e-healthcare services, Iran J. Comput. Sci. 3 (4) (2020) 195–205.
[12] A.H.M. Kamal, M.M. Islam, Enhancing the embedding payload by handling the affair of association and mapping of block pixels through prediction errors histogram, in: 2016 International Conference on Networking Systems and Security (NSysS), IEEE, 2016.
[13] W. Hong, Adaptive reversible data hiding method based on error energy control and histogram shifting, Opt. Commun. 285 (2012) 101–108.
[14] H. Yao, C. Qin, Z. Tang, Y. Tian, Improved dual-image reversible data hiding method using the selection strategy of shiftable pixels' coordinates with minimum distortion, Signal Process. 135 (2016) 26–35.
[15] S. Yi, Y. Zhou, Binary-block embedding for reversible data hiding in encrypted images, Signal Process. 133 (2017) 40–51.
[16] A.H.M. Kamal, M.M. Islam, Enhancing the performance of the data embedment process through encoding errors, Electronics (Basel) 5 (4) (2016) 79.
[17] A.H.M. Kamal, M.M. Islam, Facilitating and securing offline e-medicine service through image steganography, Healthc. Technol. Lett. 1 (2) (2014) 74–79.
[18] M.D. Hasan, M.A.M. Amin, S.T. Mahdi, Steganalysis techniques and comparison of available softwares, Cyberspace (2020).
[19] C.F. Lee, W. C-Y, C. K-C, An efficient reversible data hiding with reduplicated exploiting modification direction using image interpolation and edge detection, Multimed. Tools Appl. (2016).
[20] S. Kumar, A. Singh, M. Kumar, Information hiding with adaptive steganography based on novel fuzzy edge identification, Defence Technol. 15 (2) (2019) 162–169.
[21] S. Sun, A novel edge based image steganography with 2^k correction and Huffman encoding, Inf. Process. Lett. (2015).
[22] C. Vanmathi, S. Prabu, Image steganography using fuzzy logic and chaotic for large payload and high imperceptibility, Int. J. Fuzzy Syst. (2017).
[23] G. Swain, Adaptive pixel value differencing steganography using both vertical and horizontal edges, Multimed. Tools Appl. 75 (21) (2016) 13541–13556.
[24] J. Bai, C.-C. Chang, T.-S. Nguyen, C. Zhu, Y. Liu, A high payload steganographic algorithm based on edge detection, Displays 46 (2017) 42–51.
[25] D.R. Setiadi, Improved payload capacity in LSB image steganography uses dilated hybrid edge detection.
[26] E.J. Kusuma, O.R. Indriani, C.A. Sari, E.H. Rachmawanto, D.R.I.M. Setiadi, An imperceptible LSB image hiding on edge region using DES encryption, in: 2017 International Conference on Innovative and Creative Information Technology (ICITTech), IEEE, 2018.
[27] S. Khan, N. Ahmad, M. Ismail, N. Minallah, T. Khan, A secure true edge based 4 least significant bits steganography, IEEE, 2015.
[28] W.J. Chen, C.C. Chang, T.H.N. Le, High payload steganography mechanism using hybrid edge detector, Expert Syst. Appl. 37 (2010).
[29] H.W. Tseng, H.S. Leng, High-paylaod block-based data hiding scheme using hybrid edge detector with minimal distortion, IET Image Process. 8 (2014).
[30] K. Gaurav, U. Ghanekar, Image steganography based on canny edge detection, dilation operator and hybrid coding, J. Inf. Secur. Appl. 41 (2018) 41–51.
[31] B. Vishnu, S.R. Sajeesh, L.V. Namboothiri, Enhanced image steganography with PVD and edge detection, in: 2020 Fourth International Conference on Computing Methodologies and Communication (ICCMC), IEEE, 2020.
[32] H. Sultana, A.H.M. Kamal, Image steganography system based on hybrid edge detector, in: 2021 24th International Conference on Computer and Information Technology (ICCIT), IEEE, 2021.
[33] D.R.I.M. Setiadi, J. Jumanto, An enhanced LSB-image steganography using the hybrid canny-sobel edge detection, Cybern. Inf. Technol. 18 (2) (2018).
[34] M.B. Brodeur, E. Dionne-Dostie, T. Montreuil, M. Lepage, The bank of standardized stimuli (BOSS), a new set of 480 normative photos of objects to be used as visual stimuli in cognitive research, PLoS ONE 5 (2010) e10773.